PERGAMON

International Journal of Solids and Structures 39 (2002) 4843–4865

INTERNATIONAL JOURNAL OF SOLIDS and STRUCTURES

www.elsevier.com/locate/ijsolstr

Statics and dynamics of structural interfaces in elasticity

D. Bigoni [a,*], A.B. Movchan [b]

[a] *Facolta di Ingegneria, Dipartimento di Ingegneria Meccanica e Strutturale, University of Trento, Via Mesiano 77, Trento 38050, Italy*
[b] *Department of Mathematical Sciences, University of Liverpool, Liverpool L693BX, UK*

Received 7 March 2002; accepted 4 July 2002

Abstract

The concept of structural interface possessing finite width and joining continuous media is presented. Mechanical effects differentiating this model from conventional zero-thickness interfaces are explored for static and dynamic problems. In the static case, the thickness of the interface introduces an additional characteristic length, providing a parameter which can serve different design needs, for instance, may be employed to obtain neutral coated inclusions. In the dynamic case, a number of effects arise, related to the inertia of the interface. In particular, examples demonstrate that the design of inertial properties of the interface may be useful to produce sharp filters of elastic waves.

Keywords: Mechanical interfaces; Composite materials; Elasticity; Inclusions; Bloch Waves

1. Introduction

Problems of mechanics involving imperfect interfaces are important in the design of adhesive joints, smart composite structures and analysis of dispersive elastic waves within layered systems. Interfaces may become crucial in different situations, for instance, in the struggle to enhance toughness of brittle materials (such as ceramics, Clegg et al., 1990) or to induce peculiar electric transport properties. A strong research effort was therefore devoted to this topic. Pioneering works on imperfect, linear interfaces were performed by Goland and Reissner (1944) and Jones and Whittier (1967). Formal proofs that a linear interface may be understood as a soft, thin elastic layer were given by Klarbring (1991), Geymonat and Krasucki (1996) and Klarbring and Movchan (1998). A classification of model problems for thin-walled elastic inclusion is povided in Movchan and Movchan (1995). Composite materials with imperfectly coated inclusions were considered by Hashin (1990, 1992), Lipton and Vernescu (1995), Benveniste and Miloh (2001) and Benveniste and Chen (2001). In the field of particle reinforced elastic materials, a peculiar behaviour may occur when an inclusion is coated with an elastic layer or an interface, namely, the inclusion may become neutral, in the sense that it does not alter the ambient linear field. Examples of this behaviour were provided by Lipton (1997), Bigoni et al. (1998) and Milton and Serkov (2000). In particular, Bigoni et al. have shown

* Corresponding author. Tel.: +39-0461-882507; fax: +39-0461-882599.
E-mail addresses: bigoni@ing.unitn.it (D. Bigoni), abm@liv.ac.uk (A.B. Movchan).

0020-7683/02/$ - see front matter
PII: S0020-7683(02)00416-X

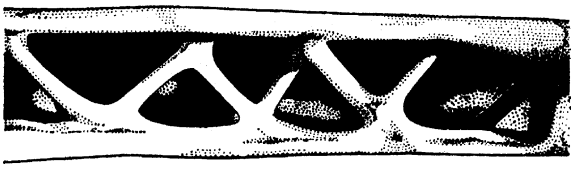

Fig. 1. Metacarpal bone from a vulture's wing; after Thompson (1942).

that stiffness parameters of the interface can be chosen in such a way that the dipole tensor associated with the inclusions can be made to be zero. To complete the discussion, it may be worth mentioning that a number of important mechanical situations involve non-linearity, which may be inherent to the constitutive law of the interface (Rice and Wang, 1989; Xu and Needleman, 1994; Falk et al., 2001) or may be a consequence of the fact that the solids joined through the interface suffer large strains (Bigoni et al., 1997; Bigoni and Gei, 2001) or may be induced by both effects (Needleman, 1990; Camacho and Ortiz, 1996; Levy, 1996).

A common characteristic of the above-mentioned models is that the thickness of the interface is zero (at least for small strain). However, thickness of a structural interface is finite, preventing the non-physical interpenetration of material occurring for compressive loads and introducing anisotropy in stiffness and inertia. A number of examples of such structures joining continuous bodies can be found in biological systems. In particular, we report in Fig. 1 a structure taken from the classical book by Thompson (1942) and [1] refer the interested reader to Gibson and Ashby (1988) and Menig et al. (2001). Biological examples suggest the possibility that assemblages of continuous bodies and structures may present definitive mechanical advantages. As an industrial counterpart of this, different technological applications can indeed be mentioned, ranging between structural engineering (Lakes, 1993), microelectromechanical systems (Elwenspoek and Wiegerink, 2001) and nanostructured materials (Gleiter, 2000).

In addition to the above-mentioned situations, a structural interface may model frictional contact between two solids (Haessig and Friedland, 1991) or a layer of strongly damaged material (see the experiments reported by Geers (1997)). The latter context was explored by Maz'ya and Hanler (1993), who have introduced an asymptotic model describing a weak non-local interface for a so-called 'disintegrating solid', in a state of anti-plane shear. The Maz'ya and Hanler model emphasises a feature characterizing a finite-thickness interface, namely, the *non-locality* of interaction between the boundaries joined through the interface.

It follows from the above discussion that if, on one hand, real structures joining continuous bodies have a finite dimension, an inertia, and peculiar anisotropic properties, on the other hand, all information regarding the microstructure are usually condensed in a zero-thickness model and all the above-mentioned features consequently neglected. In the present paper we analyze the possibility that these may play a role in a mechanical modelling. In statics, this possibility is explored solving (Section 3) the problem of an elastic circular inclusion, connected to an infinite medium through a finite-thickness interface and subject to remote, generic loading conditions. As a result, we find that the thickness of interface introduces a new characteristic length, a specific form of anisotropy and eliminates material interpenetration. In the case of dynamic problems, the analysis of wave propagation in periodic structures with interface boundaries (Sections 4–6) reveals that the effects of the interfacial inertia become crucial in determining filtering

[1] A microstructure made up of collagen fibers also exists in the periodontal ligament, the thin and soft layer attaching the cementum of the teeth to the adjacent alveolar bone. This finite-thickness, structural interface has been modelled as a zero-thickness, non-linear interface by Gei et al. (in press).

properties of the structure, which exhibits the possibility of producing remarkably narrow pass bands for elastic waves of certain type.

2. The notion of imperfect interfaces

An interface is defined 'imperfect' if either displacements or tractions (or both) can be discontinuous across it.

Interfaces of zero thickness model mechanical problems associated with cracks bridged by fibres, glide planes of dislocations in a crystal, soft and thin adhesive layers. Normally, tractions are continuous at the interface of zero thickness, namely

$$[\![\mathbf{t}]\!] = \mathbf{0}, \tag{1}$$

where the operator $[\![\cdot]\!]$ defines the jump across the interface, so that for any field ϕ defined in the bodies $+$ and $-$ connected through the interface

$$[\![\phi]\!] = \phi(\mathbf{x}_+) - \phi(\mathbf{x}_-).$$

Since a linear mass density can be regarded as zero for an interface of zero width, Eq. (1) holds true both for statics and dynamics.

When a zero-thickness interface is linear, the displacement jump $[\![\mathbf{u}]\!]$ across the interface is linearly related to components of tractions, i.e.

$$\mathbf{t} = \mathbf{C}[\![\mathbf{u}]\!], \tag{2}$$

where $\mathbf{C}$ is a second-order tensor describing the stiffness of the interface, independent of $\mathbf{u}$ and $\mathbf{t}$.

When an interface is embedded into an infinite elastic medium, a boundary value problem of static elasticity can be reduced to an integral equation posed at the interface contour Γ (see, for example, Movchan and Willis, 1996)

$$\neq\!\!\!\!\int_{\Gamma} \mathscr{L}(\mathbf{x}-\mathbf{x}')[\![\mathbf{u}]\!](\mathbf{x}')\,\mathrm{d}\mathbf{x}' + \mathbf{t}(\mathbf{u};\mathbf{x}) = \mathbf{p}, \tag{3}$$

where $\mathbf{p}$ is a given external load and matrix $\mathscr{L}$ is defined in Appendix A in the case of plane strain problems.

Interfaces of finite width may involve the jumps of tractions and effects of inertia in dynamic problems. These interfaces are non-local, in the sense that they pose constraints between different points of a continuous medium. We introduce here the concept of quasi-local interfaces to model a particular class of interfacial structures. A quasi-local interface sets prescriptions between points on opposite sides of the interface and corresponding to each other through a given law. This law will be simple in the examples presented in the following—for instance, points lying on the same normal line to the interface will be involved for rectilinear or circular interfaces—but it seems not difficult to extend the concept to more complicated geometries.

In order to explain the behaviour of a quasi-local interface, we begin with the simple example sketched in Fig. 2 of a two-dimensional microstructure joining two continuous media and mimicking the biologic structure reported in Fig. 1. In particular, we consider two elastic solids subjected to plane strain deformation and a discrete structure of bars, defined for unit out-of-plane length. The bars are inclined at an angle α (β) with respect to the interface (normal) and have length l (Fig. 2). We assume that the angle β (Fig. 2) is small, so that the tangential stiffness of the interface is also small.

An elementary cell—consisting of two bars connecting two bodies, as shown in the particular of Fig. 2—can be considered to evaluate the stiffness of the interface. In particular, the components $N_x^{(3)}$, $N_y^{(3)}$ of the

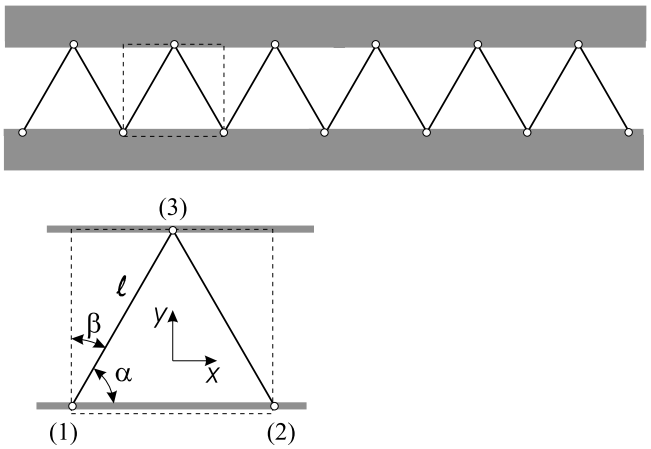

Fig. 2. Interfacial microstructure.

force acting on the node (3) of the structure (an opposite force acts on the solid connected through the interface) can be represented in the form

$$\begin{aligned} N_x^{(3)} &= \frac{EA}{l}\left(-u_x^{(1)}\cos^2\alpha - u_y^{(1)}\frac{\sin 2\alpha}{2} + 2u_x^{(3)}\cos^2\alpha - u_x^{(2)}\cos^2\alpha + u_y^{(2)}\frac{\sin 2\alpha}{2}\right), \\ N_y^{(3)} &= \frac{EA}{l}\left(-u_x^{(1)}\frac{\sin 2\alpha}{2} - u_y^{(1)}\sin^2\alpha + 2u_y^{(3)}\sin^2\alpha + u_x^{(2)}\frac{\sin 2\alpha}{2} - u_y^{(2)}\sin^2\alpha\right), \end{aligned} \tag{4}$$

where $\alpha = \pi/2 - \beta$, $0 < \beta \ll 1$, l is the length of the bars composing the structure, E their Young modulus and A the cross section area. In the case of a weak interface, to a certain order of approximation, the bodies connected to the interface can be assumed to be rigid. In this case

$$u_x^{(1)} - u_x^{(2)} = 0 \tag{5}$$

and

$$u_y^{(2)} - u_y^{(1)} = 2\theta l\cos\alpha, \tag{6}$$

where θ is the (small) angle of relative rigid-body rotation of the solids connected through the interface. Consequently, the term

$$\frac{1}{2}\left(u_y^{(2)} - u_y^{(1)}\right)\sin 2\alpha$$

is of order $O(\theta\beta^2)$ and will be neglected. As a result, a simple condition of contact across the interface is obtained

$$\begin{pmatrix} N_x^{(3)} \\ N_y^{(3)} \end{pmatrix} = \frac{2EA}{l}\begin{bmatrix} \beta^2 & 0 \\ 0 & 1-\beta^2 \end{bmatrix}\begin{pmatrix} u_x^{(3)} - U_x \\ u_y^{(3)} - U_y \end{pmatrix}, \tag{7}$$

where $\mathbf{U} = (\mathbf{u}^{(1)} + \mathbf{u}^{(2)})/2$. Eq. (7) represents the constitutive equation of the interface, whereas equilibrium of the unit cell structure imposes continuity of force $\mathbf{N}^{(3)}$, i.e. of resultant forces across the interface. The stiffness matrix which appears in (7) corresponds to a material of low resistance to a shear parallel to the interface and a finite stiffness with respect to a loading orthogonal to the interface. In the limit $\beta \to 0$ the interface transmits only a normal force, cutting off shear components.

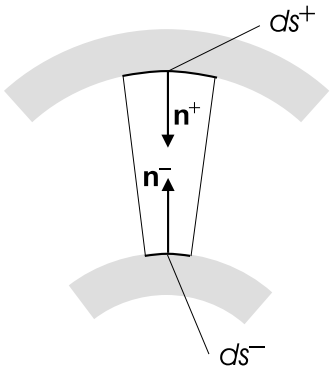

Fig. 3. Finite width interface.

In the continuum limit, the relation (7) imposes the following transmission condition

$$\langle \mathbf{t} \rangle = \mathbf{C}(\mathbf{U}^+ - \mathbf{U}^-), \tag{8}$$

where $\langle \mathbf{t} \rangle$ is the average of tractions across the interface and $\mathbf{U}^+$ and $\mathbf{U}^-$ are the values of the displacement at opposite sides of the interface; $\mathbf{C}$ is the stiffness matrix of the interface.

In addition to the constitutive relation of the interface (8), we also note that in the static case the resultant force is continuous across the interface

$$\mathbf{F}^- = \boldsymbol{\sigma}^- \mathbf{n}^- \, \mathrm{d}s^- = -\boldsymbol{\sigma}^+ \mathbf{n}^+ \, \mathrm{d}s^+ = -\mathbf{F}^+, \tag{9}$$

where $\mathbf{n}^\pm$ are the unit outward normal vectors at the interface boundaries; $\boldsymbol{\sigma}^\pm$ is the stress tensor, and $\mathrm{d}s^+$ and $\mathrm{d}s^-$ are the area elements (see Fig. 3).

It may be worth mentioning that a particular case of the interfacial constitutive law (8) and (9) has been employed by Ru (2001) to describe the van der Waals interaction between adjacent carbon nanotubes.

3. An elastic static inclusion with finite-thickness interface

A circular elastic inclusion connected to an infinite elastic matrix through a structural interface of the type specified by Eqs. (8) and (9) is solved in this section under *general* conditions at infinity. The problem setting is similar to that assumed by Bigoni et al. (1998), except that now the interface has a finite thickness (Fig. 4). Results can have different engineering applications, among which we mention the analysis of nanotubes embedded in elastic media (see the model presented by Ru (2001)).

Denoting with + quantities referred to the infinite elastic plane and with − quantities referred to the inclusion, due to the particular geometry of our problem, Eq. (9) becomes

$$\sigma_{rr}^+(R+\delta) = \sigma_{rr}^- R, \quad \sigma_{r\theta}^+(R+\delta) = \sigma_{r\theta}^- R. \tag{10}$$

The force transmitted by the interface is linearly related to the difference between displacements at corresponding points in the matrix and in the inclusion. From Eq. (8), the traction vector at the matrix interface can be expressed as:

$$\sigma_{rr}^+ = s_r[U_r^+(\boldsymbol{x}^+) - U_r^-(\boldsymbol{x}^-)], \quad \sigma_{r\theta}^+ = s_\theta[U_\theta^+(\boldsymbol{x}^+) - U_\theta^-(\boldsymbol{x}^-)], \tag{11}$$

where s_r and s_θ are the stiffnesses of the interface and $\mathbf{U}$ is the displacement vector. When the thickness of the interface is equal to zero, the well-known model of linear interface—for instance employed by

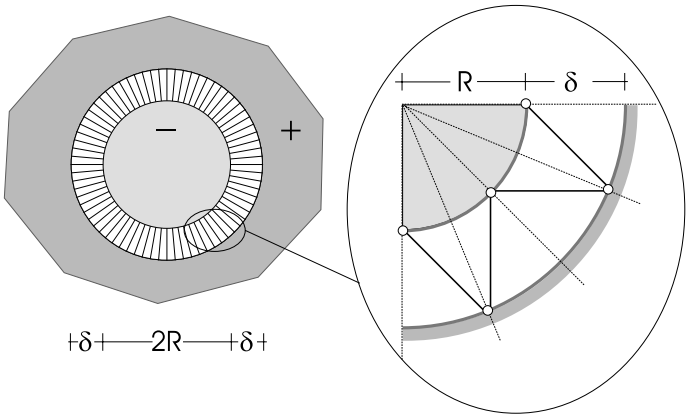

Fig. 4. Circular elastic inclusion with microstructural interface.

Bigoni et al. (1998)—is recovered. It should be important to remark that the assumed model of interface allows to avoid any further explicit consideration of the interface itself, which enters the formulation only through conditions (10) and (11). A generic displacement field is postulated at infinity:

$$\mathbf{U}^{+}(\mathbf{x}) \to \mathbf{U}^{+}_{\infty}(\mathbf{x}), \quad \text{as } \mathbf{x} \to \infty, \tag{12}$$

which is assumed to satisfy Navier's equations and to admit the representation (Sendeckyj, 1970; Yu and Sendeckyj, 1974)

$$\mathbf{U}^{+}_{\infty}(\mathbf{x}) = \{p(x_1,x_2),\ q(x_1,x_2)\}, \tag{13}$$

where p and q are order N polynomial functions of the coordinates (x_1,x_2).

The problem to be analyzed consists in finding a displacement field $\mathbf{U}$

- corresponding to (13) at infinity;
- satisfying the Navier equations

$$\mu\Delta\mathbf{U}(\mathbf{x}) + (\lambda+\mu)\nabla\nabla\cdot\mathbf{U}(\mathbf{x}) = \mathbf{0} \tag{14}$$

  in the inclusion and in the matrix (where the Lamé coefficients λ and μ are equipped with superscripts $-$ or $+$ when referred to the inclusion or to the matrix, respectively);
- satisfying, through kinematic compatibility and constitutive equations, conditions (10) and (11) at the interface.

On introducing the complex variable $z = x_1 + \mathrm{i}\,x_2$, the stress tensor and displacement vector components can be expressed in terms of the complex potentials $\varphi(z)$ and $\psi(z)$ as (Muskhelishvili, 1953):

$$\begin{aligned} &U_r + \mathrm{i}U_\theta = \frac{1}{2\mu}\mathrm{e}^{-\mathrm{i}\theta}\Big(\kappa\varphi(z) - z\overline{\varphi'(z)} - \overline{\psi(z)}\Big),\\ &\sigma_{rr} + \sigma_{\theta\theta} = 2(\varphi'(z) + \overline{\varphi'(z)}),\\ &\sigma_{\theta\theta} - \sigma_{rr} + 2\mathrm{i}\sigma_{r\theta} = 2\mathrm{e}^{2\mathrm{i}\theta}(\bar{z}\varphi''(z) + \psi'(z)), \end{aligned} \tag{15}$$

where

$$\kappa = \frac{\lambda+3\mu}{\lambda+\mu}$$

for plane strain. The complex potentials φ and ψ are analytical functions in the region where they specify the solution of the elastostatic problem, so that the solution is sought employing the following representation of the complex potentials

$$\varphi_-(z) = \sum_{k=0}^{+\infty} c_k z^k, \quad \psi_-(z) = \sum_{k=0}^{+\infty} d_k z^k, \tag{16}$$

analytic inside the disk of radius R and

$$\varphi_+(z) = \sum_{k=-\infty}^{+\infty} a_k z^k, \quad \psi_+(z) = \sum_{k=-\infty}^{+\infty} b_k z^k, \tag{17}$$

analytic in the outer region $\{\boldsymbol{x} : R+\delta < \sqrt{x_1^2+x_2^2} < +\infty\}$ and have a pole at infinity. The constants a_k, b_k are defined from the conditions at infinity (13) for $0 \leqslant k \leqslant N$. In order to rewrite the interface boundary conditions in terms of complex potentials, we note that the continuity of forces on the inner and outer boundaries of the interface corresponds to the fact that for two points of complex plane, say $z^- = R\mathrm{e}^{\mathrm{i}\theta}$ and $z^+ = (R+\delta)\mathrm{e}^{\mathrm{i}\theta}$, the following condition holds:

$$\varphi_+(z^+) + z^+\overline{\varphi'_+(z^+)} + \overline{\psi_+(z^+)} = \varphi_-(z^-) + z^-\overline{\varphi'_-(z^-)} + \overline{\psi_-(z^-)}. \tag{18}$$

Following Muskhelishvili's technique, the boundary integral equations holding in the whole plane become

$$\begin{aligned} \oint_{L_+} \frac{[\varphi_+(t) + t\overline{\varphi'_+(t)} + \overline{\psi_+(t)}]\,\mathrm{d}t}{t-z} &= \oint_{L_-} \frac{[\varphi_-(t) + t\overline{\varphi_-(t)} + \overline{\psi_-(t)}]\,\mathrm{d}t}{t-z}, \\ \oint_{L_+} \frac{[\overline{\varphi_+(t)} + \bar{t}\varphi'_+(t) + \psi_+(t)]\,\mathrm{d}t}{t-z} &= \oint_{L_-} \frac{[\overline{\varphi_-(t)} + \bar{t}\varphi'_-(t) + \psi_-(t)]\,\mathrm{d}t}{t-z}, \end{aligned} \tag{19}$$

where L_- and L_+ denote the inner and outer circular boundaries of the interface, respectively.

The system of equations (19) can be solved employing theorems on Cauchy-type integrals and the complex potentials expansion (16) and (17), thus obtaining

$$\sum_{k=-\infty}^{+\infty} a_k (z^+)^k + z^+ \sum_{k=-\infty}^{+\infty} k\overline{a}_k (\overline{z^+})^{k-1} + \sum_{k=-\infty}^{+\infty} \overline{b}_k (\overline{z^+})^k = \sum_{k=0}^{+\infty} c_k (z^-)^k + z^- \sum_{k=0}^{+\infty} k\overline{c}_k (\overline{z^-})^{k-1} + \sum_{k=0}^{+\infty} \overline{d}_k (\overline{z^-})^k. \tag{20}$$

Considering Eq. (20) on the two circles of radii R and $R+\delta$, i.e. on

$$z^+ = (R+\delta)z, \quad \overline{z^+} = \frac{R+\delta}{z}, \quad |z| = 1, \quad z^- = Rz, \quad \overline{z^-} = \frac{R}{z}, \quad |z| = 1, \tag{21}$$

one obtains

$$\begin{aligned} &\sum_{k=-\infty}^{+\infty} a_k (R+\delta)^k z^k + \sum_{k=-\infty}^{+\infty} k\overline{a}_k (R+\delta)^k z^{2-k} + \sum_{k=-\infty}^{+\infty} \overline{b}_k (R+\delta)^k z^{-k} \\ &\quad = \sum_{k=0}^{+\infty} c_k R^k z^k + \sum_{k=0}^{+\infty} k\overline{c}_k R^k z^{2-k} + \sum_{k=0}^{+\infty} \overline{d}_k R^k z^{-k}, \quad |z| = 1, \end{aligned} \tag{22}$$

which are equivalent to (20).

Collecting coefficients near the same powers of z yields the system of linear equations for the unknown coefficients a_k, b_k, c_k, d_k:

$$a_n (R+\delta)^n + (2-n)\overline{a}_{2-n}(R+\delta)^{2-n} + \overline{b}_{-n}(R+\delta)^{-n} = c_n R^n + (2-n)\overline{c}_{2-n}R^{2-n} + \overline{d}_{-n}R^{-n}, \tag{23}$$

where $n \in \mathbb{Z}$ and coefficients a_n, b_n are known for $n > 0$ from conditions at infinity, whereas coefficients c_n, d_n are equal to zero for $n < 0$.

Let us consider now the constitutive equation of the interface (11). Employing the complex potential representation, the radial and tangential components of the stress tensor can be rewritten in the following form:

$$\begin{aligned} \sigma_{rr} &= \varphi'(z) + \overline{\varphi'(z)} - \mathrm{Re}[\mathrm{e}^{2\mathrm{i}\theta}(\overline{z}\varphi''(z) + \psi'(z))], \\ \sigma_{r\theta} &= \mathrm{Im}[\mathrm{e}^{2\mathrm{i}\theta}(\overline{z}\varphi''(z) + \psi'(z))], \end{aligned} \tag{24}$$

so that the boundary conditions (11) assume the complex variable representation:

$$s_r(U_r^+ - U_r^-) + \mathrm{i}s_\theta(U_\theta^+ - U_\theta^-) = \sigma_{rr}^+ + \mathrm{i}\sigma_{r\theta}^+. \tag{25}$$

Re-writing condition (25) in terms of Cauchy integrals, taking its series expansion, writing the result on the two circles of radii R and $R + \delta$ and collecting terms near the same power of z, yields the following system of linear equations (see Appendix B for details)

$$\begin{aligned} &\frac{s_r + s_\theta}{4\mu_+}(\kappa_+ a_{n+1}(R+\delta)^{n+1} - (1-n)\overline{a}_{1-n}(R+\delta)^{1-n} - \overline{b}_{-n-1}(R+\delta)^{-n-1}) \\ &\quad - \frac{s_r + s_\theta}{4\mu_-}(\kappa_- c_{n+1}R^{n+1} - (1-n)\overline{c}_{1-n}R^{1-n} - \overline{d}_{-n-1}R^{-n-1}) + \frac{s_r - s_\theta}{4\mu_+}(\kappa_+ \overline{a}_{1-n}(R+\delta)^{1-n} - (n+1)a_{n+1} \\ &\qquad \times (R+\delta)^{n+1} - b_{n-1}(R+\delta)^{n-1}) - \frac{s_r - s_\theta}{4\mu_-}(\kappa_- \overline{c}_{1-n}R^{1-n} - (n+1)c_{n+1}R^{n+1} - d_{n-1}R^{n-1}) \\ &\quad = (n+1)a_{n+1}(R+\delta)^n + (1-n^2)\overline{a}_{1-n}(R+\delta)^{-n} + (n+1)\overline{b}_{-n-1}(R+\delta)^{-n-2}, \end{aligned} \tag{26}$$

where the index n ranges between $-N-1$ and $N-1$, moreover, coefficients a_n and b_n for $n > 0$ are known from condition at infinity, and $c_n = d_n = 0$ for $n < 0$.

We are now in a position to solve the linear system of equations (23) and (26), thus obtaining the complex potentials coefficients, solution of our problem and reported in Appendix C.

It can be observed from the solution, coefficients (C.1), that:

- the interface introduces an additional length scale in the problem, namely, the interface thickness δ;
- the thickness δ of the interface results to be always summed to the radius R of the inclusion;
- the solution corresponding to the zero-thickness interface is recovered when $\delta = 0$.

The result obtained above, holding for generic conditions at infinity, yields an immediate evaluation of the effect of unphysical overlapping of matrix and inclusion materials occurring in the zero-thickness interface model, where the interface is subject to compressive tractions. In order to avoid the overlapping, in fact, it is sufficient that the thickness of the interface be greater than the absolute value of the minimum negative radial displacement jump across the interface. Under the assumed hypotheses of infinitesimal theory of elasticity, this displacement jump is however very small (compared, say, to the radius of the inclusion), so that a small interface thickness may compensate any possible overlapping.

3.1. Homogeneous stress field at infinity

The case when an homogeneous deformation is prescribed at infinity, corresponds to a linearly varying displacement field and to the well-known Eshelby problem. In this case, the general expression for the complex potentials becomes

$$\varphi_+(z) = a_1 z + a_{-1}z^{-1}, \quad \psi_+(z) = b_1 z + b_{-1}z^{-1} + b_{-3}z^{-3}, \quad \varphi_-(z) = c_1 z + c_3 z^3, \quad \psi_-(z) = d_1 z, \tag{27}$$

where coefficients a_1 and b_1 are related to the conditions at infinity through:

$$\begin{aligned}
&a_1 = \frac{\alpha\mu_+}{\kappa_+ - 1}, \quad b_1 = -\alpha\mu_+, \quad \text{when } \mathbf{U}_\infty = (\alpha x_1, 0),\\
&a_1 = \frac{\beta\mu_+}{\kappa_+ - 1}, \quad b_1 = \beta\mu_+, \quad \text{when } \mathbf{U}_\infty = (0, \beta x_2),\\
&a_1 = 0, \quad b_1 = \mathrm{i}\sqrt{2}\gamma\mu_+, \quad \text{when } \mathbf{U}_\infty = \frac{\gamma}{\sqrt{2}}(x_2, x_1),
\end{aligned} \tag{28}$$

with $\alpha, \beta, \gamma \in \mathbb{R}$. Coefficients a_{-1}, b_{-1}, b_{-3}, c_1, c_3, d_1 can be obtained from the general expressions reported in Appendix C and result to be given by

$$\begin{aligned}
a_{-1} &= \frac{\overline{b}_1(R+\delta)^2}{D_2}\Big\{s_r s_\theta (R+\delta)^2 \Gamma_-^+(\mu_- - \mu_+) + (s_r + s_\theta)(R+\delta)\mu_+\mu_-(3(\mu_- - \mu_+) - \Gamma_-^+) - 12\mu_+^2\mu_-^2\Big\},\\
b_{-1} &= 2\mathrm{Re}(a_1)(R+\delta)^2 \frac{s_r(R+\delta)(\mu_-(\kappa_+ - 1) - \mu_+(\kappa_- - 1)) - 4\mu_+\mu_-}{s_r(R+\delta)(\mu_+(\kappa_- - 1) + 2\mu_-) + 4\mu_+\mu_-},\\
b_{-3} &= \frac{\overline{b}_1(R+\delta)^4}{D_2}\Big\{s_r s_\theta (R+\delta)^2 \Gamma_-^+(\mu_- - \mu_+) - (R+\delta)\mu_+\mu_-(s_r + s_\theta)(\Gamma_-^+ - 3\mu_- + 3\mu_+)\\
&\quad - (R+\delta)\mu_+\mu_-(s_r - s_\theta)(\Gamma_+^- + \mu_- - \mu_+) - 12\mu_+^2\mu_-^2\Big\},\\
c_1 &= \frac{\mathrm{Re}(a_1)(R+\delta)^2 s_r(\kappa_+ + 1)\mu_-}{R[4\mu_+\mu_- + s_r(R+\delta)(\mu_+(\kappa_- - 1) + 2\mu_-)]} + \mathrm{i}\frac{\mathrm{Im}(a_1)(R+\delta)(\kappa_+ + 1)\mu_-}{R(\kappa_- + 1)\mu_+},\\
c_3 &= \frac{b_1(R+\delta)^2(s_\theta - s_r)(\kappa_+ + 1)\mu_-^2\mu_+}{R^3 D_2},\\
d_1 &= \frac{b_1(R+\delta)^2(\kappa_+ + 1)\mu_-(s_r s_\theta (R+\delta)\Gamma_-^+ + 6 s_r\mu_+\mu_-)}{R D_2},
\end{aligned} \tag{29}$$

where

$$\Gamma_+^- = \mu_+ + \mu_-\kappa_+, \quad \Gamma_-^+ = \mu_- + \mu_+\kappa_-$$

and

$$D_2 = s_r s_\theta \Gamma_+^-\Gamma_-^+(R+\delta)^2 + (s_r + s_\theta)(R+\delta)(3\Gamma_+^- + \Gamma_-^+)\mu_+\mu_- + 12\mu_+^2\mu_-^2.$$

As in the case of the zero-thickness interface (Gao, 1995; Bigoni et al., 1998), Eshelby's statement that the deformation field is homogeneous inside the inclusion, holds if $c_3 = 0$, a condition occurring when the stiffness in radial and tangential directions are equal, $s_r = s_\theta$.

The coefficient a_{-1} associated with the dipole field controls the perturbation of the dilatation in the elastic matrix. The parameters of the interface can be chosen in such a way that $a_{-1} = 0$ and hence the inclusion becomes neutral with respect to the dilatation in the elastic matrix. The above statement follows from the fact that for sufficiently large $\mu_- > \mu_+$ and small values of s_r and s_θ, the quantity a_{-1} is negative, whereas for large values of δ the same quantity can be made positive. Since a_{-1} is a continuous function, it vanishes for some set of values of parameters associated to the interface.

4. Interfaces in dynamics

It may appear natural to consider that a structural interface of finite width possesses an *inertia*. This affects the dynamic response of the interface and, as will be shown in the following, may produce interesting mechanical behaviours. These are investigated through systematic examples that will be developed in the following. We begin considering a periodic elastic system made up of weak and strong layers, where the weak layers play the role of the thick interfaces. For the sake of simplicity we restrict the analysis to anti-plane shear of the periodic structure composed of isotropic elastic alternate layers $\Xi^{(0)}_{(j)}$ and $\Xi^{(1)}_{(j)}$ ($j \in \mathbb{Z}$) as shown in Fig. 5.

The thickness, mass density and shear muduli of the layers are denoted by $d^{(s)}$, $\rho^{(s)}$, $\mu^{(s)}$ ($s = 0, 1$), respectively. Moreover, we introduce the thickness d of two layers $d = d^{(0)} + d^{(1)}$ and the ratio ε between the two shear moduli $\varepsilon = \mu^{(0)}/\mu^{(1)}$. Time-harmonic vibrations of the structure are considered, so that the displacement amplitude functions $u^{(s)}_{(j)}$, with $s = 0, 1$, and $j \in \mathbb{Z}$ satisfy the following equations within the layers

$$\mu^{(s)}\nabla^2 u^{(s)}_{(j)} + \rho^{(s)}\omega^2 u^{(s)}_{(j)} = 0, \quad \text{in } \Xi^{(s)}_{(j)}; \quad s = 0, 1, \ j \in \mathbb{Z} \tag{30}$$

and the following conditions at the interfaces between elements (j)

$$u^{(0)}_{(j)} = u^{(1)}_{(j)}, \quad \mu^{(0)}\frac{\partial u^{(0)}_{(j)}}{\partial x} = \mu^{(1)}\frac{\partial u^{(1)}_{(j)}}{\partial x}, \quad j \in \mathbb{Z}. \tag{31}$$

In addition to the above equations, we assume that the displacement satisfies the quasi-periodicity condition (or Bloch condition) which is common for problems involving travelling time-harmonic waves within periodic structures:

$$u^{(s)}_{(j+1)}(x + d) = \mathrm{e}^{\mathrm{i}hd}u^{(s)}_{(j)}(x), \quad (s-1)d^{(0)} + jd < x < sd^{(1)} + jd, \tag{32}$$

where $s = 0, 1$; $j \in \mathbb{Z}$ and h is the given Bloch parameter. Assuming that the wave propagates in the direction of the x-axis, the problem becomes unidimensional and Eq. (30) reduces to

$$\mu^{(s)}\left(u^{(s)}_{(j)}\right)'' + \rho^{(s)}\omega^2 u^{(s)}_{(j)} = 0, \tag{33}$$

(in which $s = 0, 1$; $j \in \mathbb{Z}$) so that the functions $u^{(s)}_{(j)}$ can be written as

$$u^{(s)}_{(j)} = A^{(s)}_{(j)}\mathrm{e}^{\mathrm{i}\alpha^{(s)}\omega x} + B^{(s)}_{(j)}\mathrm{e}^{-\mathrm{i}\alpha^{(s)}\omega x}, \quad (s-1)d^{(0)} + jd < x < sd^{(1)} + jd, \tag{34}$$

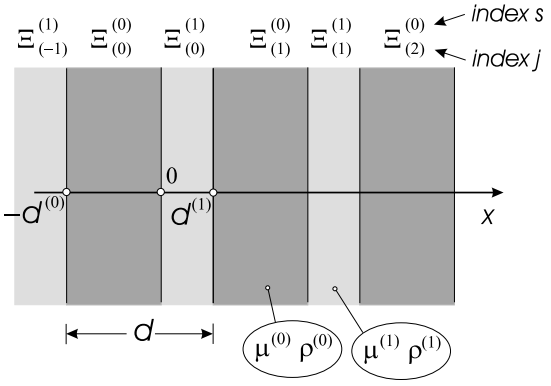

Fig. 5. Layered structure subject to harmonic anti-plane shearing.

where $s = 0, 1$; $j \in \mathbb{Z}$ and

$$\alpha^{(s)} = \sqrt{\frac{\rho^{(s)}}{\mu^{(s)}}}, \quad s = 0, 1.$$

All the coefficients $A^{(s)}_{(j)}$ and $B^{(s)}_{(j)}$ may be determined recursively imposing quasi-periodicity (32), *except four*. These may be obtained imposing continuity of displacement and traction, Eq. (31), between the two domains $\Xi^{(0)}_{(0)}$ and $\Xi^{(1)}_{(0)}$ and the two domains $\Xi^{(1)}_{(0)}$ and $\Xi^{(0)}_{(1)}$. Using (32), these boundary conditions yield the homogeneous system

$$\mathscr{M}\left\{A^{(0)}_{(0)}, A^{(1)}_{(0)}, B^{(0)}_{(0)}, B^{(1)}_{(0)}\right\}^{\mathrm{T}} = \mathbf{0}, \tag{35}$$

where

$$\mathscr{M} = \begin{bmatrix} 1 & -1 & 1 & -1 \\ k_0\varepsilon & -k_1 & -k_0\varepsilon & k_1 \\ \mathrm{e}^{\mathrm{i}(hd-k_0d^{(0)})} & -\mathrm{e}^{\mathrm{i}k_1d^{(1)}} & \mathrm{e}^{\mathrm{i}(hd+k_0d^{(0)})} & -\mathrm{e}^{-\mathrm{i}k_1d^{(1)}} \\ k_0\varepsilon\mathrm{e}^{\mathrm{i}(hd-k_0d^{(0)})} & -k_1\mathrm{e}^{\mathrm{i}k_1d^{(1)}} & -k_0\varepsilon\mathrm{e}^{\mathrm{i}(hd+k_0d^{(0)})} & k_1\mathrm{e}^{-\mathrm{i}k_1d^{(1)}} \end{bmatrix} \tag{36}$$

and

$$k_0 = \omega\alpha^{(0)}, \quad k_1 = \omega\alpha^{(1)}.$$

System (35) has a non-trivial solution if and only if matrix $\mathscr{M}$ is singular

$$\det\mathscr{M} = 0, \tag{37}$$

a condition which represents the dispersion equation relating ω and h and can be written in the form

$$\omega^2\left\{2\varepsilon\alpha^{(0)}\alpha^{(1)}\left[\cos(dh) - \cos(\omega d^{(0)}\alpha^{(0)})\cos(\omega d^{(1)}\alpha^{(1)})\right] + \left(\varepsilon^2(\alpha^{(0)})^2 + (\alpha^{(1)})^2\right)\sin(\omega d^{(0)}\alpha^{(0)})\sin(\omega d^{(1)}\alpha^{(1)})\right\} = 0. \tag{38}$$

Let us consider now the low-frequency approximation, corresponding to small values of $\omega d^{(0)}\alpha^{(0)}$ and $\omega d^{(1)}\alpha^{(1)}$

$$\begin{aligned} \omega^2\Bigg\{ & -2\varepsilon[1-\cos(dh)] + \omega^2\left(d^{(1)}(\alpha^{(1)})^2 + \varepsilon d^{(0)}(\alpha^{(0)})^2\right)(d^{(0)} + \varepsilon d^{(1)}) \\ & - \frac{\omega^4}{12}\left[\varepsilon\left(d^{(0)}\alpha^{(0)}\right)^2 + d^{(1)}(\alpha^{(1)})^2(2d^{(0)} + \varepsilon d^{(1)})\right]\left[\left(d^{(1)}\alpha^{(1)}\right)^2 + d^{(0)}(\alpha^{(0)})^2(d^{(0)} + 2\varepsilon d^{(1)})\right]\Bigg\} = 0. \end{aligned} \tag{39}$$

Direct computations performed for the Eq. (38) show the presence of a band gap on the dispersion diagram, in the case of high contrast of elastic properties of the layers. In particular, the frequency ω (non-dimensionalized through multiplication by d and $\alpha^{(0)}$) is reported versus the Bloch parameter h (multiplied by d) in Fig. 6, relative to the values $\varepsilon = 0.01$, $\alpha^{(1)}/\alpha^{(0)} = 0.1$, $d/d^{(0)} = 4$.

We may observe that the presence of the band gap at low frequency can be related to the effect of inertia of the weak interface layer $\Xi_{(1)}$.

As noted by Movchan et al. (in press), for the low-frequency approximation the Eq. (39) can be directly related to the two-masses discrete chain, representing a diatomic crystal structure in solid state physics (Brillouin, 1969; Kittel, 1971). In particular, instead of layers 1 and 2, we introduce a chain of particles of mass m_1 and m_2 connected by springs of stiffness c and representing the diatomic crystal structure (Fig. 7). The displacements u_s and v_s of the different particles from their position of equilibrium satisfy the equation of motion

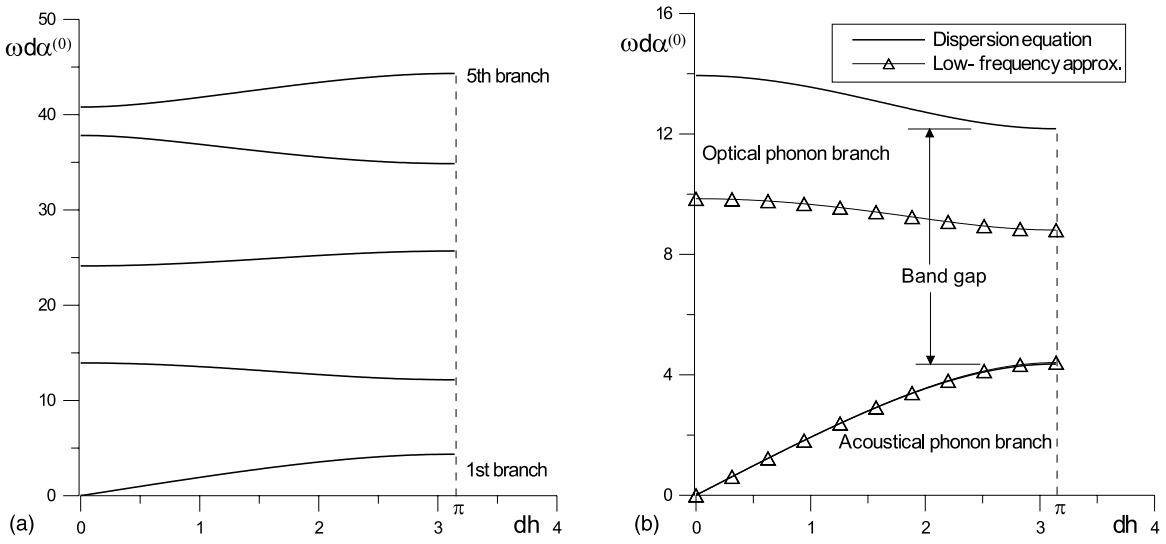

Fig. 6. Dispersion curves for $\varepsilon = 0.01$, $\alpha^{(1)}/\alpha^{(0)} = 0.1$ and $d/d^{(0)} = 4$. (a) First five branches; (b) first two branches.

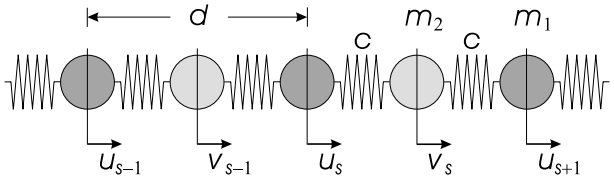

Fig. 7. Diatomic crystal structure.

$$\begin{aligned} m_1\ddot{u}_s &= c(v_s + v_{s-1} - 2u_s), \\ m_2\ddot{v}_s &= c(u_s + u_{s+1} - 2v_s) \end{aligned} \tag{40}$$

and the following quasi-periodicity condition

$$u_{s+1} = e^{ihd}u_s, \quad v_{s+1} = e^{ihd}v_s, \tag{41}$$

with d being the period of the array. Assuming the time-harmonic vibration of the system with a radian frequency ω (i.e. $u(t), v(t) \propto \exp i\omega t$), the following dispersion equation relating the Bloch parameter h and the frequency ω is obtained

$$m_1 m_2 \omega^4 - 2c(m_1 + m_2)\omega^2 + 2c^2[1 - \cos(hd)] = 0, \tag{42}$$

which, for positive ω, reproduces Eq. (39) derived for the low-frequency approximation of the continuum system. Matching of the coefficients in (39) and (42) yields the constants m_1/c and m_2/c in the form

$$\frac{m_1 m_2}{c^2} = \frac{1}{12\varepsilon}\left[\varepsilon(d^{(0)}\alpha^{(0)})^2 + d^{(1)}(\alpha^{(1)})^2(2d^{(0)} + \varepsilon d^{(1)})\right]\left[(d^{(1)}\alpha^{(1)})^2 + d^{(0)}(\alpha^{(0)})^2(d^{(0)} + 2\varepsilon d^{(1)})\right],$$
$$\frac{2(m_1 + m_2)}{c} = \frac{1}{\varepsilon}\left(d^{(1)}(\alpha^{(1)})^2 + \varepsilon d^{(0)}(\alpha^{(0)})^2\right)(d^{(0)} + \varepsilon d^{(1)}). \tag{43}$$

We note from (43) that, when ε is small, the masses m_1 and m_2 become large, so that the inertia of the weak layer contributes toward the stop band on the dispersion diagram.

It may be anticipated that a model more elaborated than the simple diatomic structure of Fig. 7 may yield a more intriguing dynamic behaviour than the above. The analysis of such a model is the focus of Section 5.

5. Comparative analysis of inertial and non-inertial interfaces

5.1. Transmission conditions

We begin with the discussion of contact conditions in dynamics for the cases of a zero-thickness non-inertial interface and for an interface of finite thickness, possessing a non-zero mass and hence inertia.

In particular, the transmission conditions for a zero-thickness interface have the same form both for statics and dynamics, Eqs. (1) and (2), whereas a quasi-local, finite width interface has a finite mass density and possesses some inertia. In this case the tractions may suffer jumps across the interface. To describe this in simple terms, we consider the semi-discrete model sketched in Fig. 8. Here, concentrated masses are connected through springs of stiffness c to continuous elements, say, elastic rods. The position of the generic mass is singled out by coordinate v_s measured from the position of equilibrium. The system of two springs and a concentrated mass is regarded as a structural interface joining continuous elements.

The forces acting on the boundaries of the sth interface are given by

$$F_- = c(v_s - u(0)), \quad F_+ = c(u(d - d^{(0)}) - v_s), \tag{44}$$

where function u denotes displacements of all points of continuous elements, referred to a common origin placed at the left side of the sth interface. The equation of motion of the mass m is

$$F_+ - F_- = m\ddot{v}_s. \tag{45}$$

Hence, the jump in tractions across the interface is

$$[\![t]\!] = F_+ - F_- = m\ddot{v}_s \tag{46}$$

and the jump in displacement across the interface is

$$[\![u]\!] = u(d - d^{(0)}) - u(0) = c^{-1}(F_+ + F_-) = 2c^{-1}\langle t\rangle. \tag{47}$$

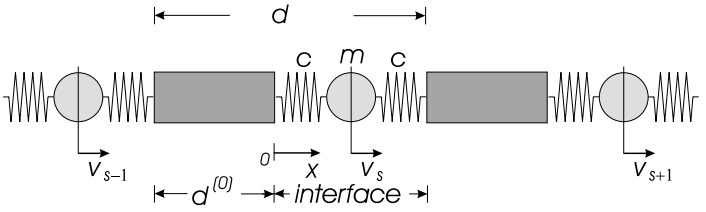

Fig. 8. Interfacial microstructure, with concentrated mass.

5.2. Wave propagation

Let us consider now propagation of elastic time-harmonic waves along the semi-discrete structure shown in Fig. 8. The amplitude of the displacement within an elastic rod satisfies the equation

$$u''(x) + \omega^2\alpha^2 u(x) = 0, \tag{48}$$

where α^{-1} is the wave speed within the rod and ω is the radian frequency. The amplitude V of vibration for the mass m is introduced as a solution of the equation

$$-\frac{m}{c}\omega^2 V = u(0) + u^{(0)}(-d^{(0)}\mathrm{e}^{\mathrm{i}hd} - 2V), \tag{49}$$

where c is the stiffness of the springs and h is a Bloch parameter associated with a propagating wave. Using the Bloch condition, the forces acting at the ends of the rod at the left-side of the interface are given in the form

$$\mu\frac{\partial u}{\partial x}\bigg|_{x=0} = c(V - u(0)) \tag{50}$$

and

$$-\mu\frac{\partial u}{\partial x}\bigg|_{x=-d^{(0)}} = c(V\mathrm{e}^{-\mathrm{i}hd} - u(-d^{(0)})), \tag{51}$$

where μ is now the longitudinal stiffness of the elastic rod.

Representing a solution of (48) by the formula

$$u = A_1\cos(\omega\alpha x) + A_2\sin(\omega\alpha x) \tag{52}$$

and using (50) and (51) we arrive at the following linear algebraic system

$$\mathscr{B}\begin{pmatrix} A_1 \\ A_2 \\ V \end{pmatrix} = 0, \tag{53}$$

where

$$\mathscr{B} = \begin{pmatrix} \mathrm{i}\omega\alpha + 2\frac{c}{\mu} & -\mathrm{i}\omega\alpha + 2\frac{c}{\mu} & -\frac{2c}{\mu} \\ \mathrm{e}^{-\mathrm{i}\omega\alpha d^{(0)}}(\mathrm{i}\omega\alpha - \frac{2c}{\mu}) & \mathrm{e}^{\mathrm{i}\omega\alpha d^{(0)}}(-\mathrm{i}\omega\alpha - \frac{2c}{\mu}) & \frac{2c}{\mu}\mathrm{e}^{-\mathrm{i}hd} \\ 1 + \mathrm{e}^{\mathrm{i}(hd - \omega\alpha d^{(0)})} & 1 + \mathrm{e}^{\mathrm{i}(hd + \omega\alpha d^{(0)})} & -2 + \frac{m\omega^2}{2c} \end{pmatrix}. \tag{54}$$

The dispersion equation has the form

$$\det\mathscr{B}(h,\omega) = 0, \tag{55}$$

which has the following equivalent representation

$$2\alpha\frac{c}{\mu}\left\{\cos(dh) - \left(1 - \frac{m\omega^2}{c}\right)\cos(\alpha d^{(0)}\omega)\right\} + \omega\left\{\frac{mc}{\mu^2} + \alpha^2\left(2 - \frac{m\omega^2}{c}\right)\right\}\sin(\alpha d^{(0)}\omega) = 0 \tag{56}$$

for positive ω and h.

5.3. Eigenvalues and eigenvectors

Numerical solutions of the dispersion equation (56) are presented below, which evidence the influence of interfacial inertia on the dispersion diagrams. A detailed analysis is also included of 'trapped modes', representing the standing waves within the structure.

The dispersion diagrams describing $\omega = \omega(dh)$ (normalized through multiplication by $d^{(0)}$ and α) are presented in Fig. 9 for $d^{(0)}c/\mu = 0.5$, moreover, Fig. 9(a) is relative to $m/(\mu d^{(0)}\alpha^2) = 0.5$, whereas inertia of the interface is set equal to zero, $m = 0$, in Fig. 9(b). It can be immediately observed from the figures that the presence of inertia results in an additional dispersion curve, corresponding to a narrow band centered at around $\omega d^{(0)}\alpha \approx 2$ and representing a so-called 'optical mode'. This becomes evident in Fig. 10, where the direct comparison of (a) and (b) is reported. It is clear that the effect of inertia consists of a small perturbation of the branches on diagram (b), plus an additional optical mode on the diagram (a).

The low frequency stop bands, characterizing waves that cannot propagate through the periodic structure, are indicated in Fig. 9. We note that the presence of the mass m creates a 'tunneling effect' at a frequency $\omega \in (\omega_B, \omega_C)$ (Fig. 9); this creates a filter of elastic waves which would enable one to transmit a signal within a narrow range of frequencies. Filters of this type might be efficient in the design of acoustic lasers (the so-called 'sasers', Makler et al., 1996; Zavtrak and Volkov, 1996).

Points A, B, C and D on the dispersion diagram relative to Fig. 9(a) are associated with standing waves that exist at the edges of the band gap intervals. The eigenvectors relative to those points provide information on the relative wave modes. In particular, on introducing the vector $\boldsymbol{\beta} = (A_1, A_2, V)$, the computed values of the eigenvectors associated to points A, B, C and D are

$$\boldsymbol{\beta}_A = (0.887, -0.462, 0), \quad \boldsymbol{\beta}_B = (0.240, 0.205, 0.949),$$
$$\boldsymbol{\beta}_C = (-0.140, 0.256, 0.956), \quad \boldsymbol{\beta}_D = (-0.989, 0.144, 0)$$

showing that vibrations associated with A and D correspond to motions within elastic rods, whereas the eigenvectors $\boldsymbol{\beta}_B$ and $\boldsymbol{\beta}_C$ correspond to vibrations associated to the inertia of the interface.

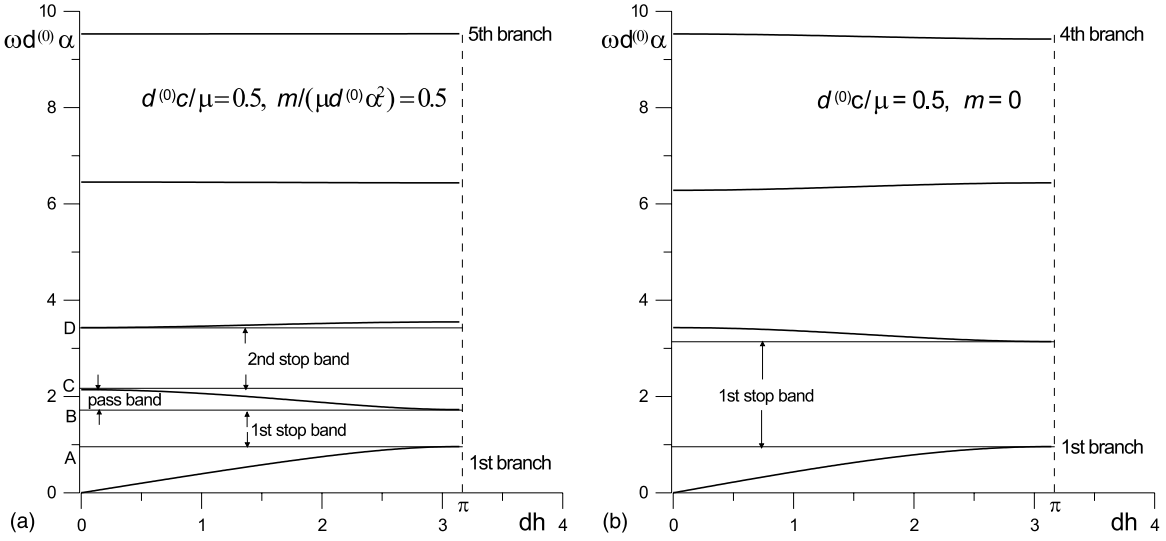

Fig. 9. Dispersion curves for $d^{(0)}c/\mu = 0.5$. (a) Inertial interface $m/(\mu d^{(0)}\alpha^2) = 0.5$; (b) interface without inertia, $m = 0$.

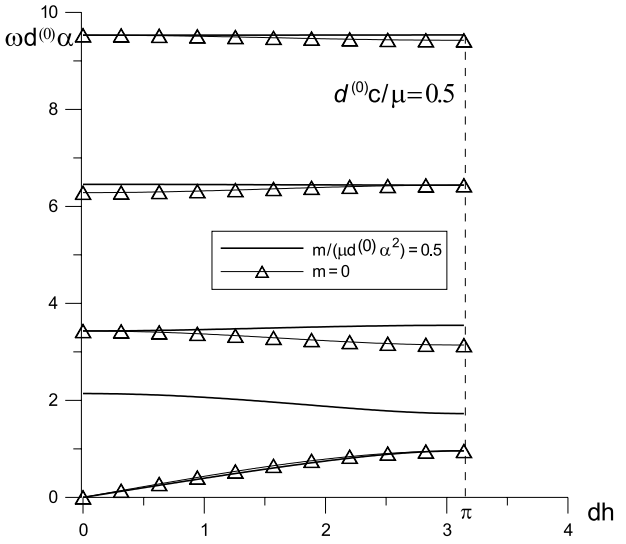

Fig. 10. Dispersion curves for $d^{(0)}c/\mu = 0.5$. Comparison between inertial interface, $m/(\mu d^{(0)}\alpha^2) = 0.5$, and interface without inertia, $m = 0$.

5.4. Comparison with the continuum model

The model of inertial interface shown in Fig. 8 can be considered as a higher accuracy approximation (compared to the diatomic chain reported in Fig. 7) of the layered structure sketched in Fig. 5. Assuming that $\omega > 0$ and expanding Eq. (38) for small values of $\omega d^{(1)}\alpha^{(1)}$ we obtain

$$2\varepsilon\alpha^{(0)}\alpha^{(1)}\left\{\cos(hd) - \left(1 - \frac{(\omega d^{(1)}\alpha^{(1)})^2}{2}\right)\cos(\omega d^{(0)}\alpha^{(0)})\right\} + \{(\varepsilon\alpha^{(0)})^2 + (\alpha^{(1)})^2\}\omega d^{(1)}\alpha^{(1)}\left(1 - \frac{(\omega d^{(1)}\alpha^{(1)})^2}{6}\right)\sin(\omega d^{(0)}\alpha^{(0)}) = 0, \tag{57}$$

a dispersion equation having the same structure as Eq. (56). In order to match coefficients of Eqs. (56) and (57), we assume

$$\alpha = \alpha^{(0)}, \quad \frac{m}{c(\alpha d^{(0)})^2} = \frac{1}{2}\left(\frac{d^{(1)}\alpha^{(1)}}{d^{(0)}\alpha^{(0)}}\right)^2 \tag{58}$$

and set the quantity $d^{(0)}c/\mu$ equal to a positive root of the second-order polynomial in χ:

$$\frac{m}{c(\alpha d^{(0)})^2}\chi^2 - \frac{1}{\varepsilon}\left[\varepsilon^2 + \left(\frac{\alpha^{(1)}}{\alpha^{(0)}}\right)^2\right]\frac{d^{(1)}}{d^{(0)}}\chi + 2 = 0. \tag{59}$$

Comparison of dispersion diagrams for the semi-discrete system with inertial interface (Fig. 8) and the continuum system (Fig. 5) are reported in Fig. 11. The examples refer to $\alpha^{(1)}/\alpha^{(0)} = 0.1$, $d/d^{(0)} = 4$ and $\varepsilon = 0.01$ in the case of Fig. 11(a), whereas $\varepsilon = 0.003$ in Fig. 11(b). Using Eq. (58) and selecting the largest root of Eq. (59), the above parameters are obtained for the semi-discrete system $m/[c(\alpha d^{(0)})^2] = 0.045$, and $d^{(0)}c/\mu = 66.667$ in the case of Fig. 11(a) and $d^{(0)}c/\mu = 222.222$ for Fig. 11(b).

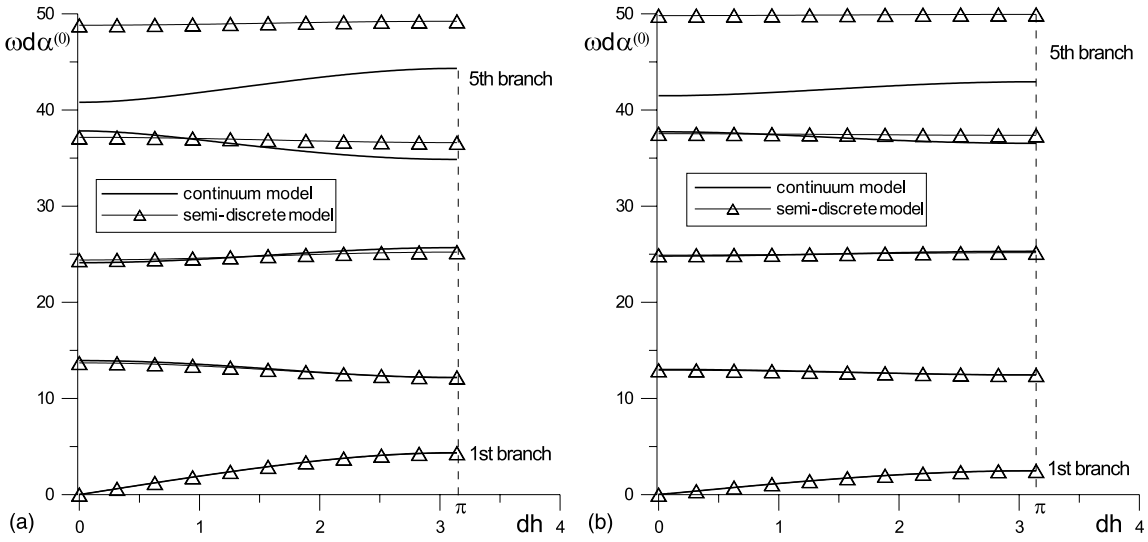

Fig. 11. Dispersion curves for continuum ($\alpha^{(1)}/\alpha^{(0)} = 0.1$, $d/d^{(0)} = 4$) and semi-discrete models ($m/[c(\alpha d^{(0)})^2] = 0.045$). (a) Dispersion curves relative to $\varepsilon = 0.01$ and $d^{(0)}c/\mu = 66.667$. (b) Dispersion curves relative to $\varepsilon = 0.003$ and $d^{(0)}c/\mu = 222.222$.

The results in the figures evidence that the accuracy of the approximation increases when values of the parameter ε become small. The semi-discrete model reproduces the acoustic and optical modes to a high accuracy and provides a correct structure of the whole dispersion diagram within a wide range of frequencies.

6. A structural interface as a sharp filter for elastic waves

The simple structural interface model introduced in Section 5 is employed below to design a sharp filter for elastic waves. Let us consider, in particular, the periodic structure shown in Fig. 12, where we analyze shear and pressure waves propagating in the direction of the x-axis.

The structure consists of elastic layers with mass density ρ alternate to rigid layers with mass density m and connected to these through a structure similar to that sketched in Fig. 2. Due to the particular propagation condition considered here, the analysis can be performed within the frame of the one-dimensional

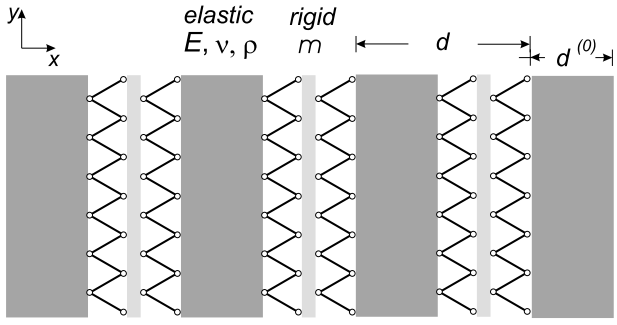

Fig. 12. Structural interface model for a periodic, two-dimensional structure.

model of inertial interface shown in Fig. 8. We employ the following parameters describing propagation of longitudinal and transverse waves: the Young modulus is $E = 200$ GPa, the Poisson ratio is $v = 0.3$, and the mass density is $\rho = 7800$ kg/m^3; the geometrical parameters (see Fig. 2) are

$$\delta = 0.2, \quad \alpha = 1.37, \quad l = 0.5 \text{ m}, \quad A = 0.1 \text{ m (area per unit length)}, \quad d_0 = 1 \text{ m},$$

finally, the mass per unit out-of-plane area of the rigid layer within the interface is $m = 1000$ kg/m^2. The stiffness coefficients and the wave speeds are given by

$$\mu_1 = \mu = 7.69 \times 10^7 \text{ Pa}, \quad c_1 = \frac{2EA\delta^2}{l}\frac{1}{2l\cos\alpha} = 1.6 \times 10^7 \text{ Pa/m}, \quad \alpha_1^{-1} = \sqrt{\frac{\mu}{\rho}} = 99.3 \text{ m/s}$$

for transverse waves, and

$$\mu_2 = 2\mu + \lambda = 2.69 \times 10^8 \text{ Pa}, \quad c_2 = \frac{2EA(1-\delta^2)}{l}\frac{1}{2l\cos\alpha} = 3.8 \times 10^8 \text{ Pa/m},$$

$$\alpha_2^{-1} = \sqrt{\frac{2\mu + \lambda}{\rho}} = 185.8 \text{ m/s}$$

for longitudinal waves; here $\mu = E/(2(1+v)), \lambda = Ev/((1+v)(1-2v))$ are the Lamé elastic moduli.

Pressure and shear modes are presented in Fig. 13, whereas Fig. 14 refers to the same set of parameters as in Fig. 13, but the mass of the interface is neglected, so that the interface has no inertia. It is shown that when inertia of the interface is not present (Fig. 14) the system is characterised by a wide pass band for pressure waves at low frequencies, whereas the shear waves have a wide stop band within the range of frequencies ≈63–312 Hz. The inertial interface changes qualitatively these dispersion diagrams (Fig. 13), so that the pressure waves are not transmitted within the interval ≈7–281 Hz, whereas a narrow pass band has been created for shear waves of ≈167–186 Hz. Hence, different applications of structures of the type

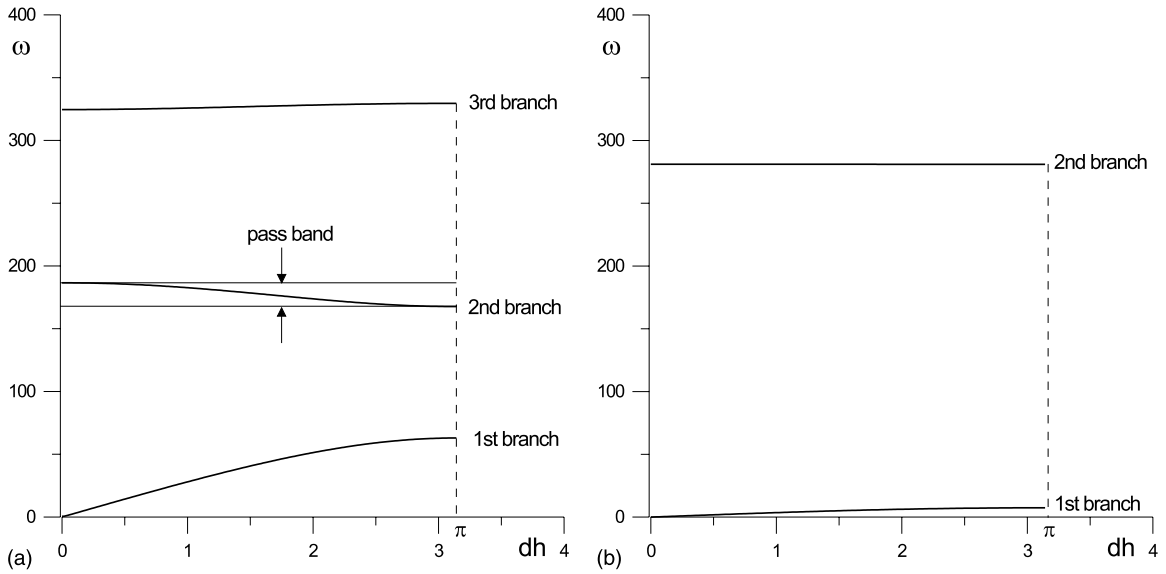

Fig. 13. Dispersion curves for the inertial interface model (Fig. 12). (a) Shear mode and (b) pressure mode dispersion diagrams.

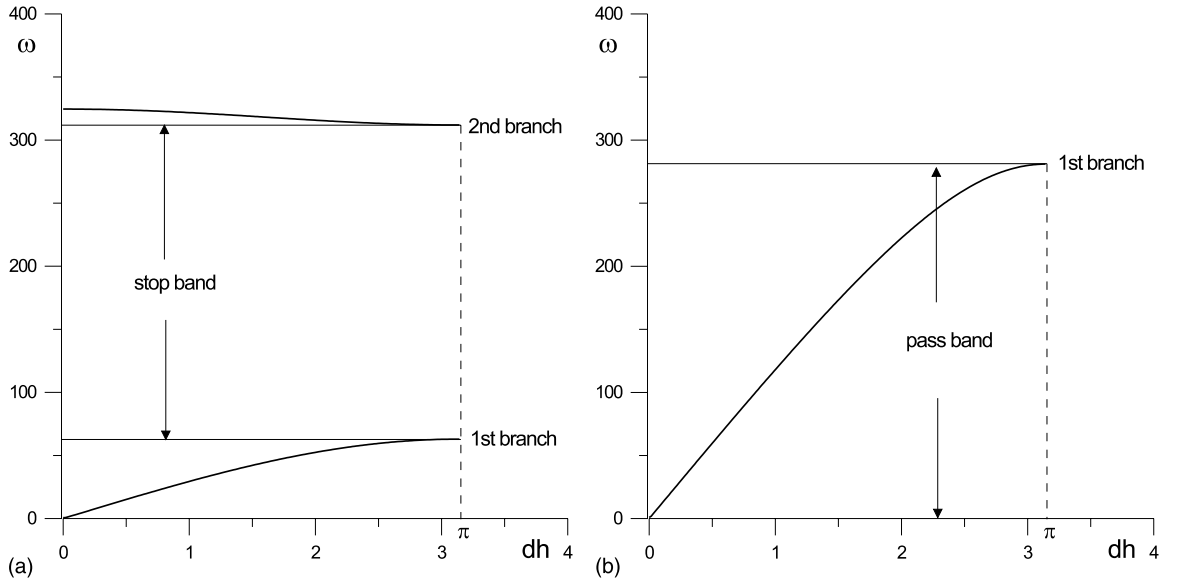

Fig. 14. Dispersion curves for the inertial interface model (Fig. 12), but involving interfaces of zero mass. (a) Shear mode and (b) pressure mode dispersion diagrams.

considered here can be advocated, for instance, in the field of vibration insulation or in creating sharp filters for elastic signals, which might be used in the design of acoustic lasers (sasers).

7. Conclusions

A novel concept of structural interface has been proposed in the present paper. This interface possesses a finite width and an inertia. Both these features influence behaviour of stress and displacements in composite structures. Our examples show that for static problems the thickness of interface introduces an additional structural parameter, whereas in dynamics the effect of inertia becomes important in the evaluation of transport properties of elastic structures. Comparison between discrete and continuous structures reveals important features associated with low frequencies which are common to both types of structures.

Possible applications of the proposed model is the design of filters of elastic waves and acoustic lasers.

Acknowledgements

The authors are grateful to Dr. S. K. Serkov (University of Utah, USA) for assistance with calculations relative to the problem of circular inclusion.

This work was performed while A.B.M. was a visiting professor at Trento University. A.B.M. would like to thank the Department of Mechanical and Structural Engineering of the University of Trento for financial support and warm hospitality. D.B. wishes to acknowledge the financial support of University of Trento.

Appendix A. Components of the kernel matrix $\mathscr{L}$

For plane strain elastic problems, the matrix $\mathscr{L}$ has the components

$$\begin{aligned}
\mathscr{L}_{11} &= \mu^2\left(\frac{\partial^2 G_{11}}{\partial x_2^2} + 2\frac{\partial^2 G_{12}}{\partial x_1 \partial x_2} + \frac{\partial^2 G_{22}}{\partial x_1^2}\right),\\
\mathscr{L}_{12} &= \mathscr{L}_{21} = \mu(\lambda+2\mu)\left(\frac{\partial^2 G_{12}}{\partial x_2^2} + \frac{\partial^2 G_{22}}{\partial x_1 \partial x_2}\right) + \lambda\mu\left(\frac{\partial^2 G_{12}}{\partial x_1^2} + \frac{\partial^2 G_{11}}{\partial x_1 \partial x_2}\right),\\
\mathscr{L}_{22} &= (\lambda+2\mu)^2\frac{\partial^2 G_{22}}{\partial x_2^2} + 2\lambda(\lambda+2\mu)\frac{\partial^2 G_{12}}{\partial x_1 \partial x_2} + \lambda^2\frac{\partial^2 G_{11}}{\partial x_1^2},
\end{aligned} \tag{A.1}$$

where the Green's tensor is

$$G_{ij}(\mathbf{x}) = -\frac{\kappa}{2\pi\mu(1+\kappa)}\left(\delta_{ij}\log|\mathbf{x}| - \kappa^{-1}\frac{x_i x_j}{\mathbf{x}^2}\right) \tag{A.2}$$

in which $\kappa = (\lambda+3\mu)/(\lambda+\mu)$ and λ and μ are the Lamé elastic moduli, so that taking derivatives yields

$$\begin{aligned}
\mathscr{L}_{11} &= -\frac{2\mu}{\pi(1+\kappa)}\left(\frac{1}{\mathbf{x}^2} - 8\frac{x_1^2 x_2^2}{\mathbf{x}^6}\right),\\
\mathscr{L}_{12} &= \mathscr{L}_{21} = -\frac{4\mu}{\pi(1+\kappa)}\frac{x_1 x_2(x_1^2 - 3x_2^2)}{\mathbf{x}^6},\\
\mathscr{L}_{22} &= -\frac{2\mu}{\pi(1+\kappa)}\left(\frac{1}{\mathbf{x}^2} + 4\frac{x_1^2 x_2^2 - x_2^4}{\mathbf{x}^6}\right).
\end{aligned} \tag{A.3}$$

Appendix B. From Eq. (25) to Eq. (26)

In terms of Cauchy integrals, condition (25) takes the form:

$$\begin{aligned}
&\frac{s_r+s_\theta}{4\mu_+}\oint_{L_+}\frac{\mathrm{e}^{-\mathrm{i}\theta}(\kappa_+\varphi_+(t) - t\overline{\varphi'_+(t)} - \overline{\psi_+(t)})\,\mathrm{d}t}{t-z} - \frac{s_r+s_\theta}{4\mu_-}\oint_{L^-}\frac{\mathrm{e}^{-\mathrm{i}\theta}(\kappa_-\varphi_-(t) - t\overline{\varphi'_-(t)} - \overline{\psi_-(t)})\mathrm{d}t}{t-z}\\
&\quad + \frac{s_r-s_\theta}{4\mu_+}\oint_{L_+}\frac{\mathrm{e}^{\mathrm{i}\theta}(\kappa_+\overline{\varphi_+(t)} - \bar{t}\varphi'_+(t) - \psi_+(t))\,\mathrm{d}t}{t-z} - \frac{s_r-s_\theta}{4\mu_-}\oint_{L_-}\frac{\mathrm{e}^{\mathrm{i}\theta}(\kappa_-\overline{\varphi_-(t)} - \bar{t}\varphi'_-(t) - \psi_-(t))\,\mathrm{d}t}{t-z}\\
&= \oint_{L_+}\frac{[\varphi'_+(t) + \overline{\varphi'_+(t)} - \mathrm{e}^{-2\mathrm{i}\theta}(t\overline{\varphi''_+(t)} + \overline{\psi'_+(t)})]\,\mathrm{d}t}{t-z}, \quad \frac{s_r+s_\theta}{4\mu_+}\oint_{L_+}\frac{\mathrm{e}^{\mathrm{i}\theta}(\kappa_+\overline{\varphi_+(t)} - \bar{t}\varphi'_+(t) - \psi_+(t))\,\mathrm{d}t}{t-z}\\
&\quad - \frac{s_r+s_\theta}{4\mu_-}\oint_{L^-}\frac{\mathrm{e}^{\mathrm{i}\theta}(\kappa_-\overline{\varphi_-(t)} - \bar{t}\varphi'_-(t) - \psi_-(t))}{t-z} + \frac{s_r-s_\theta}{4\mu_+}\oint_{L_+}\frac{\mathrm{e}^{-\mathrm{i}\theta}(\kappa_+\varphi_+(t) - t\overline{\varphi'_+(t)} - \overline{\psi_+(t)})\,\mathrm{d}t}{t-z}\\
&\quad - \frac{s_r-s_\theta}{4\mu_-}\oint_{L^-}\frac{\mathrm{e}^{-\mathrm{i}\theta}(\kappa_-\varphi_-(t) - t\overline{\varphi'_-(t)} - \overline{\psi_-(t)})\mathrm{d}t}{t-z} = \oint_{L_+}\frac{[\varphi'_+(t) + \overline{\varphi'_+(t)} - \mathrm{e}^{2\mathrm{i}\theta}(\bar{t}\varphi''_+(t) + \psi'_+(t))]\,\mathrm{d}t}{t-z}.
\end{aligned} \tag{B.1}$$

Taking the series expansion of (B.1) and writing it on the two circles of radii R and $R+\delta$, i.e. employing conditions (21), we obtain

$$\frac{s_r+s_\theta}{2}\left[\frac{1}{2\mu_+}\left(\kappa_+\sum_{j=-\infty}^{+\infty}a_j(R+\delta)^j z^{j-1}-\sum_{j=-\infty}^{+\infty}j\overline{a}_j(R+\delta)^j z^{1-j}-\sum_{j=-\infty}^{+\infty}\overline{b}_j(R+\delta)^j z^{-j-1}\right)\right.$$
$$\left.-\frac{1}{2\mu_-}\left(\kappa_-\sum_{j=0}^{+\infty}c_jR^j z^{j-1}-\sum_{j=0}^{+\infty}j\overline{c}_jR^j z^{1-j}-\sum_{j=0}^{+\infty}\overline{d}_jR^j z^{-j-1}\right)\right]+\frac{s_r-s_\theta}{2}\left[\frac{1}{2\mu_+}\left(\kappa_+\sum_{j=-\infty}^{+\infty}\overline{a}_j(R+\delta)^j z^{1-j}\right.\right.$$
$$\left.\left.-\sum_{j=-\infty}^{+\infty}ja_j(R+\delta)^j z^{j-1}-\sum_{j=-\infty}^{+\infty}b_j(R+\delta)^j z^{j+1}\right)-\frac{1}{2\mu_-}\left(\kappa_-\sum_{j=0}^{+\infty}\overline{c}_jR^j z^{1-j}-\sum_{j=0}^{+\infty}jc_jR^j z^{j-1}-\sum_{j=0}^{+\infty}c_jR^j z^{j+1}\right)\right]$$
$$=\sum_{j=-\infty}^{+\infty}ja_j(R+\delta)^{j-1}z^{j-1}+\sum_{j=-\infty}^{+\infty}j\overline{a}_j(R+\delta)^{j-1}z^{1-j}-\sum_{j=-\infty}^{+\infty}j(j-1)\overline{a}_j(R+\delta)^{j-1}z^{1-j}-\sum_{j=-\infty}^{+\infty}j\overline{b}_j(R+\delta)^{j-1}z^{-j-1}. \tag{B.2}$$

After simplification and collection of coefficients near the same power of z in (B.2), the system of linear equations (26) for the unknown coefficients is obtained.

Appendix C. Coefficients in the expansion of complex potentials

$$a_{1-n}=\frac{\overline{b}_{n-1}(R+\delta)^{2n-2}}{D_n}\{s_rs_\theta(R+\delta)^2\Gamma_-^+(\mu_--\mu_+)-4(n^2-1)\mu_+^2\mu_-^2$$
$$+(s_r+s_\theta)(R+\delta)\mu_+\mu_-[(n+1)(\mu_--\mu_+)-(n-1)\Gamma_-^+]\}$$
$$+\frac{\overline{a}_{n+1}(R+\delta)^{2n}(n+1)}{D_n}\{s_rs_\theta(R+\delta)^2\Gamma_-^+(\mu_--\mu_+)-(s_r-s_\theta)(R+\delta)(\kappa_++1)\mu_+\mu_-^2$$
$$+(s_r+s_\theta)(R+\delta)\mu_+\mu_-[(n+1)(\mu_--\mu_+)-(n-1)\Gamma_-^+]-4(n^2-1)\mu_+^2\mu_-^2\},$$
$$b_{-1}=2\mathrm{Re}(a_1)(R+\delta)^2\frac{s_r(R+\delta)(\Gamma_+^--\Gamma_-^+)-4\mu_+\mu_-}{s_r(R+\delta)(\Gamma_-^++\mu_--\mu_+)+4\mu_+\mu_-},$$
$$b_{-2}=\overline{a}_2(R+\delta)^4\frac{s_rs_\theta(R+\delta)(\kappa_+\mu_--\kappa_-\mu_+)-2(s_r+s_\theta)\mu_+\mu_-}{s_rs_\theta(R+\delta)\Gamma_-^++2(s_r+s_\theta)\mu_+\mu_-},$$
$$b_{-1-n}=\frac{\overline{b}_{n-1}(R+\delta)^{2n}(n-1)}{D_n}\left\{s_rs_\theta(R+\delta)^2\Gamma_-^+(\mu_--\mu_+)-(s_r+s_\theta)(R+\delta)\mu_+\mu_-[(\mu_+-\mu_-)(n+1)\right.$$
$$\left.+\Gamma_-^+(n-1)]+(s_\theta-s_r)(R+\delta)\mu_+\mu_-(\kappa_++1)\mu_--4(n^2-1)\mu_+^2\mu_-^2\right\}$$
$$+\frac{\overline{a}_{n+1}(R+\delta)^{2n+2}}{D_n}\left\{s_rs_\theta(R+\delta)^2[(\kappa_++1)\mu_-(\Gamma_+^--\Gamma_-^+)-n^2(\mu_+-\mu_-)\Gamma_-^+]\right.$$
$$-4n^2(n^2-1)\mu_+^2\mu_-^2+2(s_\theta-s_r)(R+\delta)(n^2-1)(\kappa_++1)\mu_+\mu_-^2$$
$$\left.-(s_r+s_\theta)(R+\delta)\mu_+\mu_-\left[2(\kappa_++1)\mu_-+n^2[(n-1)\Gamma_-^++(n+1)(\mu_+-\mu_-)]\right]\right\},$$
$$c_0=\frac{a_0\Gamma_+^-+\overline{b}_0(\mu_+-\mu_-)}{(\kappa_-+1)\mu_+}+\frac{2\overline{a}_2(R+\delta)^3s_rs_\theta(\mu_+-\mu_-)\Gamma_-^+}{(\kappa_-+1)\mu_+[s_rs_\theta(R+\delta)\Gamma_-^++2(s_r+s_\theta)\mu_+\mu_-]}$$
$$+\frac{2\overline{a}_2(R+\delta)^2\mu_+\mu_-[2(s_r+s_\theta)(\mu_+-\mu_-)+(s_r-s_\theta)(\kappa_++1)\mu_-]}{(\kappa_-+1)\mu_+[s_rs_\theta(R+\delta)\Gamma_-^++2(s_r+s_\theta)\mu_+\mu_-]},$$
$$c_1=\frac{\mathrm{Re}(a_1)(R+\delta)^2s_r(\kappa_++1)\mu_-}{R[s_r(R+\delta)(\Gamma_-^++\mu_--\mu_+)+4\mu_+\mu_-]}+\mathrm{i}\frac{\mathrm{Im}(a_1)(R+\delta)(\kappa_++1)\mu_-}{R(\kappa_-+1)\mu_+},$$

$$
\begin{aligned}
c_2 &= \frac{a_2(R+\delta)^3 s_r s_\theta(\kappa_+ + 1)\mu_-}{R^2[s_r s_\theta(R+\delta)\Gamma_-^+ + 2(s_r+s_\theta)\mu_+\mu_-]},\\
c_{n+1} &= \frac{b_{n-1}R^{-n-1}(R+\delta)^n}{D_n}(\kappa_+ + 1)\mu_+\mu_-^2(s_\theta - s_r)(n-1)\\
&\quad + \frac{a_{n+1}R^{-n-1}(R+\delta)^{n+2}(\kappa_+ + 1)\mu_-}{D_n}\big\{s_r s_\theta(R+\delta)\Gamma_+^-\\
&\quad + \mu_+\mu_-\big[-(s_r+s_\theta)(n-1) + (s_r - s_\theta)(n^2-1)\big]\big\},\\
d_0 &= \frac{b_0\Gamma_-^+ - \overline{a}_0(\kappa_+\mu_- - \kappa_-\mu_+)}{(\kappa_- + 1)\mu_+} - \frac{2a_2(R+\delta)^3 s_r s_\theta[(\kappa_- + 1)\mu_+(\kappa_+\mu_- - \kappa_-\mu_+) + (\mu_+ - \mu_-)\Gamma_-^+]}{(\kappa_- + 1)\mu_+[s_r s_\theta(R+\delta)\Gamma_-^+ + 2(s_r+s_\theta)\mu_+\mu_-]}\\
&\quad + \frac{2a_2(R+\delta)^2\mu_+\mu_-[(s_r+s_\theta)2\Gamma_-^+ - (s_r - s_\theta)(\kappa_+ + 1)\mu_-]}{(\kappa_- + 1)\mu_+[s_r s_\theta(R+\delta)\Gamma_-^+ + 2(s_r+s_\theta)\mu_+\mu_-]},\\
d_{n-1} &= \frac{b_{n-1}R^{-n+1}(R+\delta)^n(\kappa_+ + 1)\mu_-}{D_n}\big\{s_r s_\theta(R+\delta)\Gamma_-^+ + \mu_+\mu_-\big[(s_r - s_\theta)(n^2-1) + (s_r+s_\theta)(n+1)\big]\big\}\\
&\quad + \frac{a_{n+1}R^{-n+1}(R+\delta)^{n+2}(n+1)(\kappa_+ + 1)\mu_-}{D_n}\big\{s_r s_\theta(R+\delta)(\Gamma_-^+ - \Gamma_+^-)\\
&\quad + \mu_+\mu_-\big[(s_r - s_\theta)(n^2-2) + 2(s_r+s_\theta)\big]\big\},
\end{aligned}
\tag{C.1}
$$

where $n \geqslant 2$,

$$\Gamma_+^- = \kappa_+\mu_- + \mu_+, \quad \Gamma_-^+ = \kappa_-\mu_+ + \mu_-$$

and

$$D_n = s_r s_\theta(R+\delta)^2\Gamma_+^-\Gamma_-^+ + (s_r+s_\theta)(R+\delta)\mu_+\mu_-[\Gamma_+^-(n+1) + \Gamma_-^+(n-1)] + 4(n^2-1)\mu_+^2\mu_-^2.$$

References

Benveniste, Y., Chen, T., 2001. On the Saint-Venant torsion of composite bars with imperfect interfaces. Proc. R. Soc. Lond. 457, 231–255.

Benveniste, Y., Miloh, T., 2001. Imperfect soft and stiff interfaces in two-dimensional elasticity. Mech. Mater. 33, 309–323.

Bigoni, D., Gei, M., 2001. Bifurcations of a coated, elastic cylinder. Int. J. Solids Struct. 38, 5117–5148.

Bigoni, D., Ortiz, M., Needleman, A., 1997. Effect of interfacial compliance on bifurcation of a layer bonded to a substrate. Int. J. Solids Struct. 34, 4305–4326.

Bigoni, D., Serkov, S.K., Valentini, M., Movchan, A.B., 1998. Asymptotic models of dilute composites with imperfectly bonded inclusions. Int. J. Solids Struct. 35, 3239–3258.

Brillouin, L., 1969. Wave propagation and group velocity. Academic Press, New York.

Camacho, G.T., Ortiz, M., 1996. Computational modelling of impact damage in brittle materials. Int. J. Solids Struct. 33, 2899–2938.

Clegg, W.J., Kendall, K., Alford, N.McN., Button, T.W., Birchall, J.D., 1990. A simple way to make tough ceramics. Nature 347, 455–457.

Elwenspoek, M., Wiegerink, R., 2001. Mechanical microsensors. Springer-Verlag, Berlin.

Falk, M.L., Needleman, A., Rice, J.R., 2001. A critical evaluation of cohesive zone models of dynamic fracture. J. Phys. IV 11, 43–50.

Gao, Z., 1995. A circular inclusion with imperfect interface: Eshelby's tensorand related problems. J. Appl. Mech. 62, 860–866.

Geers, M.G.D., 1997. Experimental analysis and computational modelling of damage and fracture. Ph.D. Thesis, Technische Universiteit Eindhoven.

Gei, M., Genna, F., Bigoni, D., in press. An interface model for the periodontal ligament. J. Biomech. Eng., ASME.

Geymonat, G., Krasucki, F., 1996. A limit model of a soft, thin joint. In: Marcellini, P., Talenti, G., Vesentini, E. (Eds.), Partial Differential Equations and Applications. Marcel Dekker, New York, pp. 165–173.

Gibson, L.J., Ashby, M.F., 1988. Cellular Solids—Structure and Properties. Pergamon Press, Oxford.

Gleiter, H., 2000. Nanostructured materials: basic concepts and microstructure. Acta Mater. 48, 1–29.

Goland, M., Reissner, E., 1944. The stresses in cemented joints. J. Appl. Mech., A17–A27.
Haessig, D.A., Friedland, B., 1991. On the modeling and simulation of friction. J. Dynamic Sys., Measur. Control, ASME 113, 355–362.
Hashin, Z., 1990. Thermoelastic properties of fiber composites with imperfect interface. Mech. Mater. 8, 333–348.
Hashin, Z., 1992. Extremum principles for elastic etherogeneous media with imperfect interfaces and their application to bounding of effective moduli. J. Mech. Phys. Solids 40, 767–781.
Jones, J.P., Whittier, J.S., 1967. Waves at a flexibly bonded interface. J. Appl. Mech. 34, 905–909.
Kittel, C., 1971. Introduction to solid state physics, fourth ed. Wiley & Sons, New York.
Klarbring, A., 1991. Derivation of a model of adhesively bonded joints by the asymptotic expansion method. Int. J. Eng. Sci. 29, 493–512.
Klarbring, A., Movchan, A.B., 1998. Asymptotic modelling of adhesive joints. Mech. Mater. 28, 137–145.
Lakes, R., 1993. Materials with structural hierarchy. Nature 361, 511–515.
Levy, A.J., 1996. The effective dilatational response of fiber-reinforced composites with nonlinear interface. J. Appl. Mech. 63,, 357–364.
Lipton, R., 1997. Variational methods, bounds and size effects for composites with highly conducting interface. J. Mech. Phys. Solids 45, 361–384.
Lipton, R., Vernescu, B., 1995. Variational methods, size effects and extremal microstructures for elastic composites with imperfect interface. Math. Models Meth. Appl. Sci. 5, 1139–1173.
Makler, S.S., Tuyarot, D.E., Anda, E.V., Vasilevskiy, M.I., 1996. Ultra-high-frequency coherent sound generation in resonant tunneling. Surf. Sci. 361/362, 239–242.
Maz'ya, V.G., Hanler, M., 1993. Approximation of solutions of the neumann problem in disintegrating domains. Math. Nachr. 162, 261–278.
Menig, R., Meyers, M.H., Meyers, M.A., Vecchio, K.S., 2001. Quasi-static and dynamic mechanical response of *Strombus gigas* (conch) shells. Mater. Sci. Eng., A 297, 203–211.
Milton, G.W., Serkov, S.K., 2000. Bounding the current in nonlinear conducting composites. J. Mech. Phys. Solids 48, 1295–1324.
Movchan, A.B., Movchan, N.V., 1995. Mathematical modelling of solids with nonregular boundaries. CRC Press.
Movchan, N.V., Willis, J.R., 1996. Critical load for a Mode-I crack reinforced by bridging fibres. Quart. J. Mech. Appl. Math. 49, 545–564.
Movchan, A.B., Zalipaev, V.V., Movchan, N.V., in press. Photonic band gaps for fields in continuous and lattice structures. In: Proc. IUTAM Symp. on Analytical and Computational Fracture Mechanics of Non-Homogeneous Materials, Cardiff.
Muskhelishvili, N.I., 1953. Some basic problems of the mathematical theory of elasticity. Noordhoff, Groningen.
Needleman, A., 1990. An analysis of tensile decohesion along an interface. J. Mech. Phys. Solids 38, 289–324.
Rice, J.R., Wang, J.S., 1989. Embrittlement of interfaces by solute segregation. Mater. Sci. Eng., A 107, 27–40.
Ru, C.Q., 2001. Axially compressed buckling of a doublewalled carbon nanotube embedded in an elastic medium. J. Mech. Phys. Solids 49, 1265–1279.
Sendeckyj, G.P., 1970. Elastic inclusion problems in plane elastostatics. Int. J. Solids Struct. 6, 1535–1543.
Thompson, D.W., 1942. On Growth and Form. Cambridge University Press, Cambridge.
Yu, I.W., Sendeckyj, G.P., 1974. Multiple circular inclusion problems in plane elastostatics. J. Appl. Mech. 41, 215–221.
Zavtrak, S.T., Volkov, I.V., 1996. Sound amplification by stimulated emission of radiation (Saser) with cylindrical resonator. Ultrasonic 34, 691–694.